Cellulose (2014) 21:347–356
DOI 101007/s10570-013-0159-1

ORIGINAL PAPER

Influence of drying restraint on physical and mechanical properties of nanofibrillated cellulose films

Carlos Baez · John Considine · Robert Rowlands

Received: 23 August 2013/Accepted: 21 December 2013/Published online: 4 January 2014

Abstract Nanofibrillated cellulose (NFC) is a renewable and biodegradable fibril that possesses high strength and stiffness resulting from high level hydrogen bonding. Films made from NFC shrink and distort as they transition from a wet state (20 wt% solids) to a state of moisture equilibrium (90 wt% solids at 50 % RH, 23 °C). Material distortions are driven by development of moisture gradients within the fibril network and effectively reduce mechanical performance. For this study, NFC was extracted from softwood holocellulose by first employing a chemical pretreatment [(2,2,6,6-tetramethylpiperidin-1-yl)oxyl catalyzed oxidation] followed by mechanical fibrillation using ultrasound energy. To assess the problem of film distortion, neat NFC films were dried at 50 % RH, 23 °C under one of the following three restraint conditions: fully restrained, partially restrained, and uniaxially drawn. The influence of restraint condition on the resulting physical and mechanical properties was evaluated. Raman and X-ray results showed that fibrils in the uniaxially drawn specimens tended to align with the drawing axis, whereas no in-plane orientation effects were observed for the fully or partially restrained specimens. Fully restrained specimens had a respective strength and stiffness of 222 MPa and 14 GPa in every (in-plane) direction. However, samples that were wet-drawn to a 30 % strain level had a respective strength and stiffness of 474 MPa and 46 GPa in the direction of draw. Mechanical properties for axially drawn specimens had both fibril alignment and fibril straightening contributions.

Keywords Nanofibrillated cellulose · Microfibrillated cellulose · Nanocellulose Restraint drying · Fiber orientation · Cellulose nanofibers

Introduction

Nanofibrillated cellulose (NFC) has recently become a major area of research, as it offers promising advantages as a reinforcing phase in composites materials (Cheng et al. 2007; Johnson et al. 2009; Nakagaito et al. 2005). It has the potential for replacing synthetic fibers in applications where post-use biodegradability is beneficial. This material is extracted from cellulose, the most abundant natural polymer on earth, using a variety of fiber disintegration techniques. NFC fibrils have both a high axial (crystalline) stiffness (138 GPa) (Gindl et al. 2006; Moon et al. 2011) and a low thermal expansion (0.1 ppm/K) (Nakagaito and Yano 2008),

Electronic supplementary material The online version of this article (doi: 10.1007/s10570-013-0159-1) contains supplementary material, which is available to authorized users.

C. Baez (✉) · J. Considine
Forest Products Laboratory, USDA Forest Service, One Gifford Pinchot Drive, Madison, WI 53726-2398, USA
e-mail: cbaez@fs.fed.us

R. Rowlands
University of Wisconsin–Madison, 3348 Engineering Hall, 1415 Engineering Drive, Madison, WI 53706, USA

two properties that are useful in the production of high performance composites. In addition, NFC is a recyclable, renewable, and compostable material. Possible applications range from ballistic glass technology and flexible electronic displays to structural composites.

By breaking down the structural hierarchy of plant material, it is possible to separate and obtain networks composed of nano-sized fibrils by mechanical agitation of the cellulosic bundles. In this study we will define a cellulose nanofiber (or fibril) as a collection of bonded cellulose chains that together have a diameter of about 10 nm. In addition, cellulose nanofibers contain both amorphous and crystalline regions that extend periodically along their length (Nishiyama et al. 2003). The crystalline regions consist of tight parallel chains of anhydroglucose units held together by intra-molecular hydrogen bonding (Rowell 1983), while the amorphous regions lack long-range order and thus are more accessible to chemical interaction and degeneration.

Turbak et al. (1983) were the first to patent production of microfibrillated cellulose (also known as nanofibrillated cellulose) by subjecting wood pulp to high shear stresses using a homogenizer. This process requires a high energy input of about 30,000 kWh/ton (Klemm et al. 2011), to obtain a homogeneous fibrillation, and has been shown to severely damage fibrils and decrease their length. Since then, various chemical pretreatments have been developed to improve the efficiency of the fibrillation process. One such method employs a TEMPO-oxidation reaction (Saito et al. 2007), which transforms the primary hydroxyl groups located on the surface of the cellulose fiber into charged carboxylate groups. The charged fibers repel each other, facilitating the mechanical fibrillation process (where charged cellulose fibers are disintegrated into charged nanofibers) which results in a colloidal suspension.

Analogous to paper, NFC films also shrink and distort in the process of drying given that moisture evaporation at the surface occurs at a faster rate than moisture transport within the material (Gimaker et al. 2011). In addition, moisture diffusion within cellulosic materials depends on local moisture content (Topgaard and Soderman 2001), which further contributes to the formation of moisture gradients. Film distortion occurs as these gradients develop, leading to the formation of localized stress concentrations. Consequently, mechanical performance of the NFC film would most likely deteriorate by the formation of these stress concentrations.

Relatively little has been published on mechanical properties of neat NFC films in comparison with the numerous reports on properties of NFC-reinforced composites. This is because production of thick NFC films is hindered by long filtration times caused by fibril clogging. As the suspension concentrates, the path for water transport becomes more tortuous resulting in decreasing filtration rates. NFC films have potential future application as a structural component in biocomposite materials. Therefore, it is of outmost importance to characterize the physical and mechanical properties of this material as a neat film.

The range of strength and stiffness of neat NFC films obtained from previous publications averages at 190 MPa and 11 GPa (Fukuzumi et al. 2009; Iwamoto et al. 2008; Plackett et al. 2010; Sehaqui et al. 2010; Spence et al. 2010; Syverud and Stenius 2009), and depending on the specific study, these values can deviate from the average by up to 50 %. These deviations are not surprising given the variations in pulp source and pretreatment (mechanical, chemical, or enzymatic) between the studies. Even though there are clear differences between them, the effects of drying on film property were not considered on most of these studies.

Fibril orientation plays a key role on mechanical properties of NFC films. The present study makes use of Raman scattering to measure fibril alignment within the film. Purvis and others (Purvis et al. 1973; Purvis and Bower 1974) showed that oriented polymers exhibited polarization dependence in the intensity of their Raman scattering; the Raman spectrum contained information about orientation of the structural units (monomers). Wiley and Atalla (1987) used a similar technique on oriented cellulose fibers. They found a directional character of certain vibrational modes in oriented cellulose caused by the impingement of polarized laser light. Together these studies show how Raman scattering is used to determine fiber orientation in polymeric systems. Gindl et al. (2006) evaluated the mechanical properties of uniaxially drawn Lyocell fibers obtained by dissolution and subsequent coagulation in a LiCl/*N*,*N*-dimethylacetamide solvent solution. Fiber orientation was measured by X-ray diffraction and birefringence techniques. Their results showed that for a draw level of 50 %, the modulus for the cellulose II film increased from 8.5 to 26 GPa and tensile strength increased from 201 to 396 MPa with respect to the undrawn material.

They attribute these mechanical improvements to the reorientation of cellulose II fibers along the drawing direction.

The mechanical performance of previously studied NFC films depends on the physical and chemical properties of the fiber network. These properties are determined by the selected chemical pretreatment/mechanical fibrillation of the fiber suspension and subsequent physical manipulation and drying of the NFC film. The objective of this study is to investigate how the method and level of restraint applied when drying the NFC films influences the resulting physical and mechanical properties of such films.

Materials

NFC production

Ponderosa pine wood flour (40 mesh) was used as source material. The wood flour was bleached (Wise 1945) to extract lignin, resulting in holocellulose, which contains the total polysaccharide content of the wood. Holocellulose, given its high level of hemicelluloses (40 wt% obtained by sugar analysis), was chosen for two reasons: (1) to prevent fibril coalescence, which facilitates nanofibrillation (Iwamoto et al. 2008) and (2) to reduce hornification (cross-linking via hydrogen bonding) (Wan et al. 2010) of the fibrils to improve recyclability of material. In order to make holocellulose colloidal, a TEMPO-catalyzed oxidation reaction described by Saito et al. (2009) was applied. In this reaction, cellulose primary hydroxyls are oxidized to carboxylate salts that carry a net negative charge. The negatively charged fibrils repel each other, forming a colloidal suspension that facilitates mechanical fibrillation. The holocellulose was placed in a flask and diluted to 15 g/L using 0.05 M phosphate buffer (pH 6.8). The flask was placed inside a water bath at 60 °C, then 0.016 g of TEMPO/g holocellulose and 1.13 g of $NaClO_2$/g holocellulose (80 % pure) were added followed by 0.62 g of NaClO/g holocellulose, which had been first diluted from 2 to 0.1 M using the 0.05 M phosphate buffer.

After stirring for three days, the carboxylated cellulose was filtered and washed using deionized water. The reaction yield was 65 % (the other 35 % was lost as dissolved hemicellulose and cellulose), and at this point

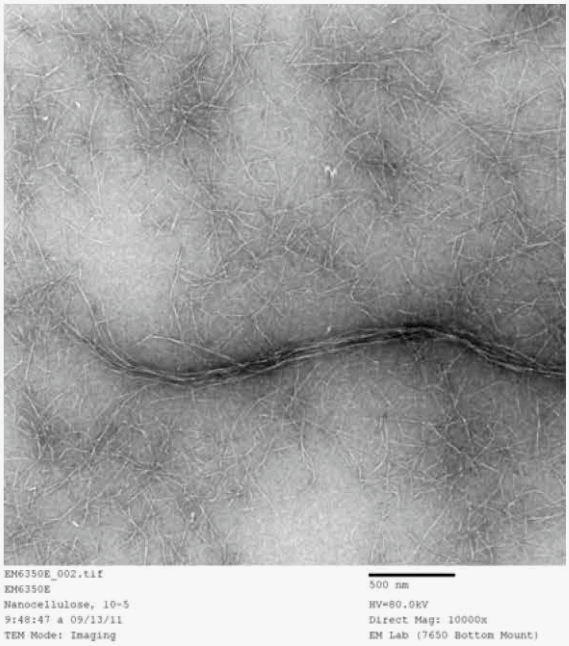

Fig. 1 TEM image of the resulting cellulose nanofiber network

the polysaccharide proportion was 80 % cellulose and 20 % hemicelluloses, as determined by sugar analysis. The carboxylate content was measured using TAPPI standard T-237 modified with higher reagent concentrations to accommodate the higher carboxyl levels and resulted in 0.5 mmol COO^-/g. The TEMPO reaction also resulted in a drop of the average degree of polymerization (DP) from 1,200 to 950 as determined using TAPPI T-230 capillary viscometer method.

Mechanical agitation is required to fully disperse and disintegrate the carboxylated cellulose fibers into nanofibers. This was accomplished using an ultrasonic probe (Sonics & Materials, Inc. model: VCX 1500 HV, Newtown, CT, USA) with a frequency of 20 kHz. Afterwards the sonicated pulp was centrifuge at 12,500g to separate the fibrillated fraction from the unfibrillated, improving suspension clarity. The sonication–centrifugation process was structured as a series of steps to balance energy consumption, suspension clarity, DP, and product yield. The result was an NFC yield of 65 % (fibrillation yield based on the carboxylated holocellulose) and a DP of 875 while consuming 8,000 kWh/ton of sonication energy plus another 4,500 kWh/ton on centrifugation.

An example of the resulting NFC product is shown in Fig. 1. The TEM image of a drop of diluted (0.1 wt%) NFC suspension reveals a network of

entangled fibrils having diameters of approximately 10 nm and lengths in the order of 1 p. Because of their disordered state, amorphous regions allow the fibrils to bend at various points along their length.

NFC films production

NFC films were produced by concentrating the suspension into a wet circular sheet using a pressure filtration chamber (YT30142HW, Millipore Corporation, Billerica, MA, USA) with applied414 kPa of air pressure in combination with a polyvinylidene fluoride filtering membrane with a pore size of 0.45 μm.

Restraint drying methods

The NFC film as removed from the filtration chamber had a solids content of approximately 20 wt%. The films were dried by one of three restraining methods:

Partially restrained (PR)

The film is placed between flexible metal screens and c-clamps are used to pin down the metallic screens against a perforated stand (see appendix in ESM). This method is intended to prevent the film from displacing out-of-plane while allowing shrinkage in the plane of the film. The diameter of the film shrinks about 20 % as the material dries and becomes denser.

Fully restrained (FR)

The NFC film is pinched between perforated metal rings to permit air flow; weights are added on top of the rings to prevent the film from slipping out (see appendix in ESM). The NFC film is prevented from in-plane shrinking by clamping the periphery of the circular film. As the film dries, this restraint causes stresses in the radial and tangential directions to develop.

Axially drawn (AD)

Rectangular samples 1.5 cm wide and 10 cm long were cut from circular film (20 wt% solids content) and clamped in a tensile test machine. Specimens were wet-drawn to a selected draw level at a displacement rate of 10 mm/min; draw levels were 1, 10, 20, 30 or 40%. After reaching the desire draw level, the specimens were left restrained in the grips to air dry at nominal 21 °C, 25 % RH. This method subjects the film to a uniaxial state of stress (see appendix in ESM). Higher levels of drawing were not studied given the high rate of specimen failure above the 40 % level. Wet-drawing of the NFC specimens has the effect of causing a decrease in width, and inversely, an increase in thickness.

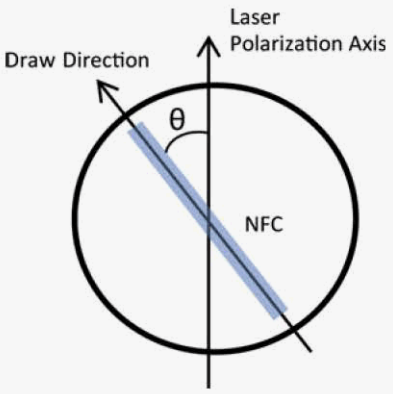

Fig. 2 Raman experimental setup

Experimental section

Raman microprobe

Raman spectra were taken using a Horiba Jobin–Yvon (USA) equipped with a linearly polarized 632.8 nm laser. Raman was used to measure and compare the degree of fibril orientation between the different restraint methods. The instrument was fitted with a rotating stage to orient the rectangular samples with respect to the axis of polarization. Measurements consisted of four repetitions each with an acquisition time of 30 s using a 50× microscope objective to focus on the surface of the sample.

The method proposed by Pleasants et al. (1998) using Raman scattering was applied here to measure fibril orientation. It works by recording the intensity ratio between the 1,094 and 1,120 cm^{-1} peak as a function of specimen orientation. These peaks are known to be sensitive to fibril orientation given that they correspond to C–Ostretching modes within the backbone of the cellulose polymer (Wiley and Atalla 1987). The set up used for this experiment is presented as a schematic in Fig. 2 showing the rectangular sample on top of the rotating stage, the polarization axis of the laser, and the angle between them. The laser

light travels perpendicular to the plane of the NFC sample.

X-ray diffraction

X-ray spectra were obtained for all samples using Bruker/Siemens Hi-Star™ 2D diffractometer featuring a monochromatic Cu Kα point source (0.8 mm) and a 1,024 pixel × 1,024 pixel area detector. The information obtained was used to construct intensity versus azimuthal angle plots to observe changes in crystalline orientation of the fibrils with respect to drying technique.

Tensile tests

Mechanical properties of the NFC films were measured with a tensile testing machine (Instron 5865, Norwood, MA, USA) equipped with a 5 kN load cell in conjunction with a MTS LX 500 noncontact laser extensometer (MTS Systems Corporation, Eden Prairie, MN, USA) to measure strain. The laser extensometer scans the specimen at a constant rate (128 Hz) and records the displacements of retroreflecting tapes adhered to the specimen at a known gage length. Samples were preconditioned in a 26 °C, 30 % RH room for 24 h and then reconditioned in 21 °C, 50 % RH room for 24 h prior to testing. A total of 2 films were made per restraint condition (and also for each drawing level) and 5 rectangular specimens were cut per film. PR and FR specimens were cut (after drying) into 1.5 cm × 10 cm tensile specimens with a nominal thickness of 70 µm, and a gage length of 5 cm was used. The AD specimens were cut into rectangles of 1.5 cm × 10 cm (at 20 % solids) and had a thickness of nominally 70 µm but dimensions changed during drawing process. Specimens were loaded at a constant grip displacement rate of 1 mm/min.

Specific stress (σ_{sp}) versus strain (ε) curves were fitted with a hyperbolic tangent model shown in Eq. (1) using an iterative numerical fitting routine. The model was obtained from Gunderson et al. (1988) and modified by adding a linear term. The parameters C_1 through C_4 are fitting constants.

$$\sigma_{sp} = C_1 \tanh(C_2(\varepsilon - C_4)) + C_3(\varepsilon - C_4) \quad (1)$$

Each of the constants has a particular influence on the shape of the model; C_1 controls the magnitude, C_2 affects the curvature at low strain, which relates to the yield strength, C_3 influences mostly the slope at high strain (linear portion), and C_4 is the strain offset. This model was used to calculate specific stiffness, E_{sp}, by evaluating the derivative of the model at zero strain.

$$E_{sp} = C_1 C_2 + C_3 \quad (2)$$

Specific toughness (U_{sp}) was calculated by numerical integration of the data from zero strain to strain at failure. Density, ρ, of individual specimens was calculated by dividing grammage, γ, by specimen thickness measured with a spherical tip micrometer (Mitutoyo Corporation, Kanagawa, Japan).

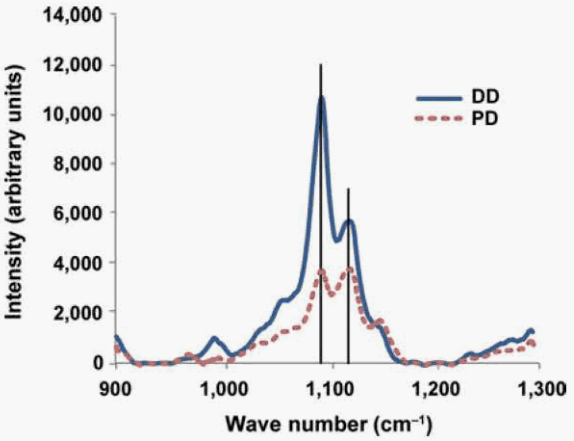

Fig. 3 Raman spectrum for 40 % axially drawn sample. DD indicates sample draw direction is aligned with laser polarization axis (θ = 0°), and PD indicates sample draw direction is perpendicular to laser polarization axis (θ = 90°)

Results and discussion

Measuring fibril orientation

Raman spectrums in the range of 900–1,300 cm^{-1} wave number were obtained for samples subjected to the various drying methods under study. The Raman spectrum for 40 % axially drawn specimen is shown in Fig. 3. Two spectra are shown, one where the draw direction is oriented parallel to the laser polarization axis (DD) and the other when the draw direction is oriented perpendicular (PD). It is clear from this plot that there is a very significant change of intensity ratio between the 1,094 and 1,120 cm^{-1} peak when probing parallel to direction of draw versus perpendicular. Although both peaks (1,094 and 1,120 cm^{-1}) exhibit

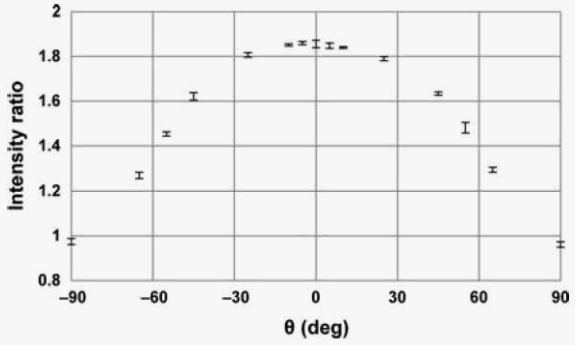

Fig. 4 Raman intensity ratio between the 1,094 and 1,120 cm ^{1} peak with respect to sample orientation (θ) for the 40 % axially drawn specimen

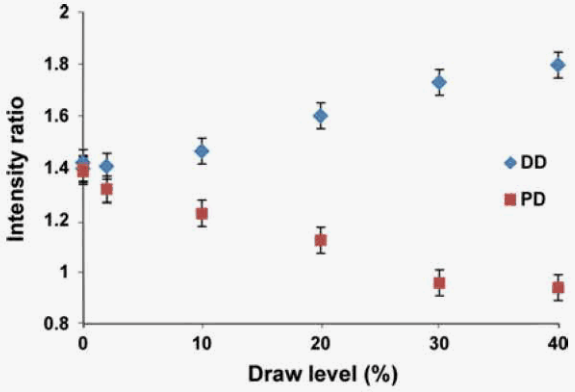

Fig. 5 Variation in Raman intensity ratio between 1,094 and 1,120 cm ^{1} with respect to draw level. Laser polarization axis is aligned either parallel to drawing direction (DD) or perpendicular to drawing direction (PD). Fully restrained and partially restrained samples are represented at 0 % draw

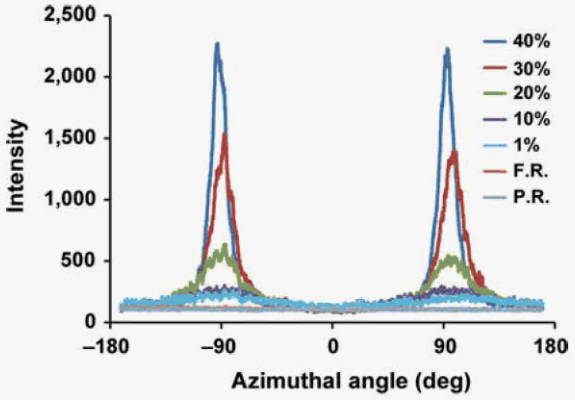

Fig. 6 X-ray diffraction (transmission mode) intensity versus azimuthal angle at (200) for all restraint drying methods studied

maximum intensity when the axis of the fibrils coincides with the polarization axis of the laser ($\theta = 0$), their intensity ratio decreases as the sample drawing axis is rotated away from the laser polarization axis ($0 < \theta < 180°$).

Evidence of fiber orientation can be seen with greater detail in Fig. 4. The plot shows how the intensity ratio between the 1,094 and 1,120 cm^{-1} varies as a function of specimen orientation (θ) for 40 % axially drawn material. The intensity ratio reaches a maximum when the DD of the specimen is oriented parallel to the laser polarization axis and gradually decreases to a minimum as the DD becomes perpendicular, i.e., $\theta = 90°$. Figure 5 presents the variation of Raman intensity ratio for the various materials. Partially and fully restrained samples had no measurable alignment. While significant increases in alignment were measured for axially drawn samples. Fiber alignment in the DD is obtained when a large fraction of fibers have their longitudinal axis orient in this direction. In this case, fibril alignment occurred as a consequence of wet drawing. The water present in the sample after removal from filtration membrane (80 wt% water) works like a plasticizer so as to significantly reduce hydrogen bonding between adjacent fibrils, creating a softer material. As a consequence, samples are able to withstand greater plastic deformation and fibrils that were once randomly oriented in the plane of the film now start to progressively align and straighten with the drawing axis as force is applied.

X-ray tests (Fig. 6) corroborated Raman results, i.e., higher drawing promoted greater crystal orientation in draw direction. For FR and PR samples scattering from the (200) occurred with equal intensity in all azimuthal directions, which reveals random crystalline orientation in these samples. In contrast, fibrils from the AD samples gradually align with the draw direction as indicated by the successive narrowing and intensification of the (200) peak.

Mechanical properties

The influence of drying methods on the tensile properties of neat NFC films was measured and the results are presented in Table 1. The average density of the specimens was 1.48 g/cm^3. Figure 7 presents stress versus strain curves for three different draw levels. In this plot, the hyperbolic tangent model was

Table 1 Tensile test results

	σ_{max}		ε_{max} %	E		U	
	kN-m/kg	MPa		kN-m/kg	GPa	kJ/kg	MJ/m^3
Fully restrained (FR)	149 (19)	222 (29)	6.1 (1.2)	9,646 (480)	14.3 (0.8)	6.3 (1.5)	9.4 (2.2)
Partially restrained (PR)	91 (6)	137 (8)	3.4 (0.6)	9,602 (540)	14.4 (0.7)	2.3 (0.6)	3.5 (0.9)
Axially drawn (AD) 1 %	238 (9)	347 (13)	8.1 (0.8)	7,083 (1,130)	10.3 (1.7)	11.4 (1.1)	16.6 (1.7)
AD 10 %	272 (14)	398 (20)	6.2 (0.8)	10,440 (365)	15.3 (0.5)	10.6 (1.8)	15.6 (2.7)
AD 20 %	315 (9)	459 (17)	4.3 (0.7)	14,158 (786)	20.6 (1.1)	8.2 (1.7)	11.9 (2.7)
AD 30 %	327 (11)	474 (21)	1.7 (0.2)	32,235 (2,158)	46.6 (2.7)	3.4 (0.6)	4.9 (0.9)
AD 40 %	[a]	[a]	[a]	40,929 (1,150)	59.5 (1.9)	[a]	[a]

The values in parenthesis indicate the standard deviation

[a] The missing values that were not possible to measure because of grip slippage at high load

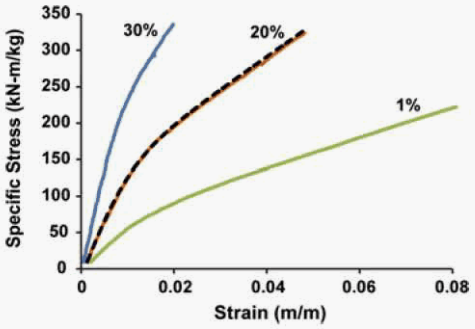

Fig. 7 Tensile stress versus strain plot for three different drawing levels. The hyperbolic tangent fit (*dashed lines*) is shown for the 20 % AD sample. *Plots* are shifted rightward for clarity

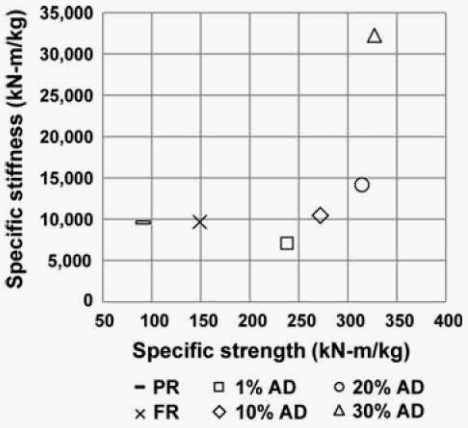

Fig. 8 Specific stiffness versus specific strength

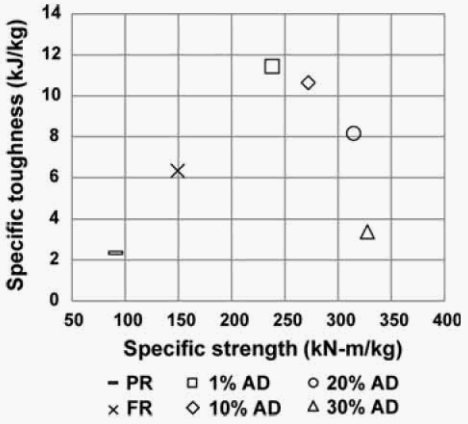

Fig. 9 Specific toughness versus specific strength

used to fit the intermediate draw level shown (20 % AD) to visualize its correspondence. In every case, the correlation coefficient (R^2) was very close to one, indicating good agreement between data and model. Specific stiffness and toughness are plotted versus specific strength in Figs. 8 and 9, respectively.

Results showed that mechanical properties of neat NFC films indeed varied with drying restraint method. In the case of the fully and partially restrained films, no change in stiffness was recorded between these two methods (Fig. 8). This is because in both cases the fiber networks were found to have no particular orientation in the plane of the film (Figs. 5, 6) and corresponds to in-plane isotropy. Although fibers for these two cases were randomly oriented, their respective recorded strengths and toughness were statistically different (Figs. 8, 9). Contrary to FR and AD samples, which remained flat, PR samples distorted as they dried because little restriction was imposed. Stress concentrations caused by material distortion ultimately reduced the maximum tensile strength and toughness of PR samples.

Film distortion is an issue that is regularly ignored in most studies involving the use of neat NFC films. This study highlights the importance of addressing film distortion as it leads to the formation of stress concentrations that tend to reduce mechanical performance. There is a study by Sehaqui et al. (2010) that also focuses on the issue of film distortion. They restrain the wet film using a vacuum sheet drier in order to produce flat and transparent MFC films (here referred as NFC films). They demonstrated superior mechanical performance from films dried by this method than by other means such as oven drying or hot pressing. It appears that drying method might in fact be an issue affecting tensile data scatter between studies of neat NFC films; a single standardized drying restraint method could in principle be followed in order to regulate these types of discrepancies.

FR samples showed lower strength and toughness than the 1 % AD samples (Table 1). It is conceivable that tensile specimens cut from the FR films develop microscopic imperfections (cracks) along the edge of the sample, given that these tensile specimens were cut after drying. The dry NFC film is stiff and brittle compared to the wet film. This would explain why the 1 % AD tensile samples, having been cut wet, had greater strength and toughness considering there is a lower chance for defects to develop at the periphery when cutting softer material.

The stiffness for a single crystalline cellulose fibril has been measured as 145 GPa (Iwamoto et al. 2009) by three point bending using AFM tip, and more recently Josefsson et al. (2013) using molecular modeling, determined the stiffness of a single cellulose fibril (having 69 % crystalline volume fraction) to be 65 GPa. However, the stiffness for NFC neat films reported in the literature fall between 5 and 18 GPa (Sehaqui et al. 2010; Iwamoto et al. 2008; Syverud and Stenius 2009; Plackett et al. 2010; Fukuzumi et al. 2009; Spence et al. 2010). In the present study, the stiffness for FR and PR film was 14 GPa, which falls within this range.

Five main reasons contribute to the stiffness disparity between the cellulose single fibril and the film: (1) low inter-fibril bonding strength, (2) random fibril orientation of the network, (3) straight versus curled fibrils, (4) stiffness of crystalline regions versus amorphous regions, and (5) film porosity. First, hydrogen bonding between cellulose fibrils is weaker and contributes less stiffness than intra-fibril hydrogen bonding occurring within the crystalline domains. This leads to inter-fibril slipping (debonding) when loading the material, which has the effect of decreasing stiffness. In addition, mechanical properties for fibrous materials that rely on inter-fiber hydrogen bonding for their cohesion will be affected in varying degrees by atmospheric humidity, as water interrupts inter-fiber bonding. Second, mechanical properties of NFC films containing randomly oriented fibrils will further decrease stiffness given that the high stiffness direction is along the longitudinal axis of the fibril. Any other conformation other than perfect fiber alignment will surely result in less than maximum stiffness. Third, a fibril can be generally aligned with the loading axis and be curled or twisted rather than straight. The curled fibril would have to straighten in order to reduce slack and reach its maximum stiffness level. Fourth, the stiffness previously reported of 145 GPa for single fibril TEMPO-oxidized tunicate cellulose (Iwamoto et al. 2009) has a crystallinity greater than 90 %. In general, NFC extracted from wood has a lower crystallinity (about 70 %, Saito et al. 2007), which further reduces the stiffness of neat NFC films from wood pulp. Finally, NFC films have a level of porosity from 10 to 20 % (Josefsson et al. 2013) that does not contribute to film stiffness and creates discontinuous voids between fibrils. The previous five points presented can be interpreted as flaws introduced into a perfectly crystalline material, which ultimately results in a fibrous material with lower symmetry and mechanical stability.

For the axially drawn NFC films, a clear pattern emerged, higher drawing levels had increased strength and stiffness coupled with a decrease in toughness (embrittlement) when probing in the direction of draw. This case corresponds to an orthotropic material, given that properties in the draw direction will in general be different from those in the perpendicular directions. Changes in mechanical properties for drawn samples were due to fiber orientation and fiber straightening effects in the direction of draw as evident from the Raman and X-ray spectra. Increasing fiber alignment along a single axis led to an increase in material stiffness in this direction. However, material toughness correlates inversely with drawing level, given that there is less fibril slack in the highly drawn specimens, diminishing strain at brake. It is possible that the highly drawn NFC (30 and 40 % AD) specimens were close to reaching a lockout point where the amorphous

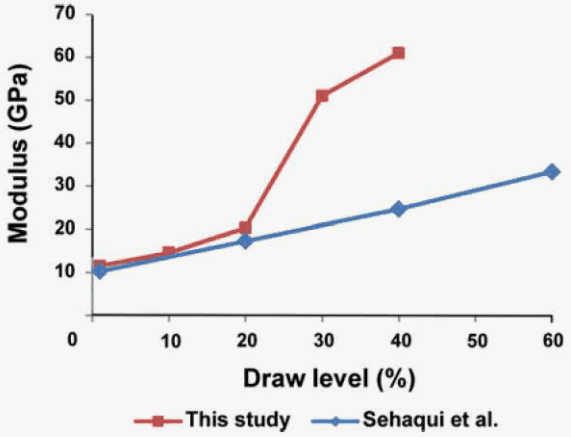

Fig. 10 Comparison of modulus versus drawing level between this study and Sehaqui et al. (2010)

material cannot continue to stretch during the wet drawing process. This idea is plausible given that the highest wet-drawing strain level that could be reached without specimen failure was about 45 %. Computer models (Nikolov et al. 2006) applied to study the behavior of semi-crystalline polymers under plastic deformation predict amorphous lockout at high strain levels. This is because semi-crystalline polymers transition from a lamellar structure to fibrillar structure at high strain levels. Therefore, given that NFC is a fibrillar material, amorphous lockout might explain the sudden jump in stiffness and drop in maximum strain (Table 1) between the 20 and 30 % AD specimens. After reducing amorphous slack (near lockout) by wet drawing at high levels, inter-fibril slip becomes the main deformation mode in NFC specimens subjected to tensile loading.

Sehaqui et al. (2012) published results from a similar study where they wet-draw TEMPO-NFC films and measured the effect on mechanical properties of the subsequently dried material. Figure 10 compares stiffness versus drawing level between studies. It is evident that values begin to deviate at higher drawing levels. A possible explanation for this difference is that strains were measured here using a laser extensometer and material stiffness was defined as the slope at zero strain of the hyperbolic tangent model [Eq. (1)], whereas in Sehaqui et al. (2012), stiffness was measured as the slope of the data at low strain, which may correspond more to a secant modulus.

In addition to fibril orientation, axial residual stresses are also expected to develop in AD films. The fibril network wants to remain in a disordered state (no directionality) given the higher number of possible disordered arrangements. Residual stresses are developed in AD specimens as work (wet-drawing) is done to orient the fibril network into a less probable state of greater order. High tensile residual stresses could ultimately limit increases in tensile strength when wet-drawing NFC films.

The objective of this study was to avoid NFC film distortion by employing restraint drying methods and to document the effect that such methods have on the physical and mechanical properties of the films. It was found that a low level of restraint (PR samples) was not enough to prevent film distortion when drying. In addition, such distortions were also found to affect the resulting mechanical properties of the film. On the other hand, high levels of restraint drying such as FR and AD samples were shown to prevent film distortion and consequently improve the mechanical properties of such films. It was also found that wet-drawing produces high gains in material stiffness along the drawing direction which enables the production of unidirectional NFC laminates.

Conclusion

This work presents the consequences produced by selected restraint drying methods on the properties of NFC films. The FR and AD methods proved to be effective in controlling film distortion, whereas the opposite was true for the PR method. Stiffness and strength of the wet-drawn NFC films increased with drawing level (in the direction of draw) while toughness and maximum strain decreased. PR films distorted to the point that stress concentrations were developed, effectively reducing tensile strength and toughness. FR films had improved mechanical properties with respect to PR films because of their flat undistorted surface. Addressing film distortion resulting from the drying of NFC films would help in reducing data scatter between studies. This study showed that drying restraint method significantly affects resulting properties because of a combination of influences, including fibril orientation, fibril straightening, and stress concentrations. This information can be used in the development of future biocomposite materials that include free-standing NFC films in their design such as ballistic glass

technology, flexible electronic displays and structural composites.

Acknowledgments TEM imaging work was funded in whole or in part with federal funds from the National Cancer Institute (NCI), National Institutes of Health (NIH), under Contract No. HHSN261200800001E. We thank Drs. S.E. McNeil, U. Baxa and their colleagues at NCI/NIH for carrying out the TEM.

References

Cheng Q, Wang SQ, Rials TG, Lee SH (2007) Physical and mechanical properties of polyvinyl alcohol and polypropylene composite materials reinforced with fibril aggregates isolated from regenerated cellulose fibers. Cellulose 14:593-602

Fukuzumi H, Saito T, Wata T, Kumamoto Y, Isogai A (2009) Transparent and high gas barrier films of cellulose nanofibers prepared by TEMPO-mediated oxidation. Biomacromolecules 10:162–165

Gimaker M, Ostlund M, Ostlund S, Wagberg L (2011) Influence of beating and chemical additives on residual stresses in paper. Nord Pulp Pap Res J 26:445-451

Gindl W, Martinschitz KJ, Boesecke P, Keckes J (2006) Changes in the molecular orientation and tensile properties of uniaxially drawn cellulose films. Biomacromolecules 7:3146–3150

Gunderson DE, Considine JM, Scott CT (1988) The compressive load-strain curve of paperboard—rate of load and humidity effects. J Pulp Pap Sci 14:J37–J41

Iwamoto S, Abe K, Yano H (2008) The effect of hemicelluloses on wood pulp nanofibrillation and nanofiber network characteristics. Biomacromolecules 91022–1026

Iwamoto S, Kai WH, Isogai A, Iwata T (2009) Elastic modulus of single cellulose microfibrils from tunicate measured by atomic force microscopy. Biomacromolecules 102571–2576

Johnson RK, Zink-Sharp A, Renneckar SH, Glasser WG (2009) A new bio-based nanocomposite: fibrillated TEMPO-oxidized celluloses in hydroxypropylcellulose matrix. Cellulose 16227–238

Josefsson G, Tanem BS, Li YJ, Vullum PE, Gamstedt EK (2013) Prediction of elastic properties of nanofibrillated cellulose from micromechanical modeling and nano-structure characterization by transmission electron microscopy. Cellulose 20761–770

Klemm D, Kramer F, Moritz S, Lindstrom T, Ankerfors M, Gray D, Dorris A (2011) Nanocelluloses: a new family of nature-based materials. Angew Chem Int Ed 50:5438–5466

Moon RJ, Martini A, Nairn J, Simonsen J, Youngblood J (2011) Cellulose nanomaterials review: structure, properties and nanocomposites. Chem Soc Rev 40:3941–3994

Nakagaito AN, Yano H (2008) The effect of fiber content on the mechanical and thermal expansion properties of biocomposites based on microfibrillated cellulose. Cellulose 15: 555–559

Nakagaito AN, Iwamoto S, Yano H (2005) Bacterial cellulose: the ultimate nano-scalar cellulose morphology for the production of high-strength composites. Appl Phys A Mater 80:93–97

Nikolov S, Lebensohn RA, Raabe D (2006) Self-consistent modeling of large plastic deformation, texture and morphology evolution in semi-crystalline polymers. J Mech Phys Solids 54:1350–1375

Nishiyama Y, Kim UJ, Kim DY, Katsumata KS, May RP, Langan P (2003) Periodic disorder along ramie cellulose microfibrils. Biomacromolecules 4:1013–1017

Plackett D, Anturi H, Hedenqvist M, Ankerfors M, Gallstedt M, Lindstrom T, Siro I (2010) Physical properties and morphology of films prepared from microfibrillated cellulose and microfibrillated cellulose in combination with amylopectin. J Appl Polym Sci 117:3601–3609

Pleasants S, Batchelor WJ, Parker IH (1998) Measuring the fibril angle of bleached fibres using micro-Raman spectroscopy. Appita J 51:373–376

Purvis J, Bower DI (1974) Study of molecular-orientation in poly(methylmethacrylate) by means of laser-Raman spectroscopy. Polymer 15:645–654

Purvis J, Bower DI, Ward IM (1973) Molecular orientation in PET studied by polarized Raman-scattering. Polymer 14: 398-400

Rowell R (1983) The chemistry of solid wood. American Chemical Society, Washington, DC

Saito T, Kimura S, Nishiyama Y, Isogai A (2007) Cellulose nanofibers prepared by TEMPO-mediated oxidation of native cellulose. Biomacromolecules 8:2485–2491

Saito T, Hirota M, Tamura N, Kimura S, Fukuzumi H, Heux L, Isogai A (2009) Individualization of nano-sized plant cellulose fibrils by direct surface carboxylation using TEMPO catalyst under neutral conditions. Biomacromolecules 101992–1996

Sehaqui H, Liu AD, Zhou Q, Berglund LA (2010) Fast preparation procedure for large, flat cellulose and cellulose/inorganic nanopaper structures. Biomacromolecules 11: 2195–2198

Sehaqui H, Mushi NE, Morimune S, Salajkova M, Nishino T, Berglund LA (2012) Cellulose nanofiber orientation in nanopaper and nanocomposites by cold drawing. ACS Appl Mater Interfaces 4:1043–1049

Spence KL, Venditti RA, Habibi Y, Rojas OJ, Pawlak JJ (2010) The effect of chemical composition on microfibrillar cellulose films from wood pulps: mechanical processing and physical properties. Bioresour Technol 101:5961–5968

Syverud K, Stenius P (2009) Strength and barrier properties of MFC films. Cellulose 16:75–85

Topgaard D, Soderman O (2001) Diffusion of water absorbed in cellulose fibers studied with H-1-NMR. Langmuir 17: 2694-2702

Turbak AF, Snyder FW, Sandberg KR (1983) Microfibrillated cellulose, a new cellulose product: properties, uses, and commercial potential. J Appl Polym Sci 37:815–827

Wan JQ, Wang Y, Xiao Q (2010) Effects of hemicellulose removal on cellulose fiber structure and recycling characteristics of eucalyptus pulp. Bioresour Technol 101: 4577-4583

Wiley JH, Atalla RH (1987) Band assignments in the Raman-spectra of celluloses. Carbohydr Res 160:113–129

Wise LE (1945) Quantitative isolation of hemicelluloses from coniferous woods: preliminary communication. Ind Eng Chem 17:63–64